Carbohydrate Polymers 271 (2021) 118405

Contents lists available at ScienceDirect

Carbohydrate Polymers

journal homepage: www.elsevier.com/locate/carbpol

Grafting PEG on cellulose nanocrystals via polydopamine chemistry and the effects of PEG graft length on the mechanical performance of composite film

Ting Zheng [a,b], Craig M. Clemons [a,c], Srikanth Pilla [a,b,d,e,*]

[a] Department of Automotive Engineering, Clemson University, Greenville, SC 29607, United States
[b] Clemson Composites Center, Clemson University, Greenville, SC 29607, United States
[c] USDA Forest Service, Forest Products Laboratory, Madison, WI 53726, United States
[d] Department of Material Science and Engineering, Clemson University, Clemson, SC 29632, United States
[e] Department of Mechanical Engineering, Clemson University, Clemson, SC 29632, United States

ARTICLE INFO

Keywords:
Natural fibre composites
Nanocrystal
Cellulose
Polydopamine
Graft length

ABSTRACT

In this study, cellulose nanocrystals (CNCs) with PEG grafts of various lengths (1 k, 2 k, 5 k, and 10 kDa) were prepared via a polydopamine (PDA) mediated method in the aqueous solution. The prepared CNC-PEGs were further used to reinforce the polyvinyl alcohol (PVA) at the loading of 0, 1, 3, 5, and 7 wt% in order to demonstrate the effects of the PEG length on the properties of the PVA/CNC nanocomposites. PEG surface modification resulted in simultaneous improvements in stiffness and toughness. The graft lengths have noticeable impacts on the properties of composites. The shorter graft yields better enhancement in strength and stiffness, attributable to the high efficiency in the stress transfer and high interface adhesion. The longer PEG graft length yields high graft-matrix entanglement, forming a thicker rubbery coating layer that enhances the toughness of PVA/CNC composites.

1. Introduction

Cellulose nanocrystals (CNCs) are a family of rod-like nanomaterials obtained by acid hydrolysis of plant-derived cellulosic pulps from wood, cotton, agricultural waste, etc. CNCs have low densities, high stiffnesses, nano-scale dimensions, and large aspect ratios and are, therefore, useful reinforcing agents for composite manufacturing. The past two decades witnessed tremendous efforts in producing high-performance CNC nanocomposites. However, a primary challenge in employing CNCs are the high hydrophilicity of CNC surface, resulting in formidable CNC aggregation when blending in hydrophobic plastics matrices, limiting composite properties (Zheng & Pilla, 2020). Methods were developed to shield CNC's original surface by adsorbing or grafting less-hydrophilic molecules. These strategies improved CNC dispersion and yielded composites of high tensile strength and stiffness, but usually at the price of composite toughness (Zheng & Pilla, 2020). The initial target of increasing CNC dispersion has now shifted to leveraging strength and toughness simultaneously by engineering a well-designed and well-defined CNC surface in order to construct robust CNC-matrix interfacial interaction. CNC surface engineering could be improved by (1) selecting an appropriate type of grafting polymer, (2) creating the proper grafting chemistry, and (3) tuning the parameters of grafts.

Introducing a polymeric rubbery coating is one approach for imparting stiff CNC with all-around performance. In brittle matrices, the polymer component can serve as a rubbery toughening agent, characterized by fine domain size, high interfacial area, low T_g (glass transition temperature), and miscibility with the matrix (Muiruri et al., 2019). A good example is CNC that is grafted with poly(D-lactide-*co*-ε-caprolactone) via ring-opening polymerization (ROP) (Muiruri et al., 2017). The graft contents (Muiruri et al., 2018) and types of end moiety (Muiruri et al., 2019) could be tuned meticulously to control the size of rubber zone and the rubber-matrix interaction. Such an approach has been used to successfully toughen poly(L-lactide) (PLA). Unfortunately, increases in strength and stiffness were not found in these studies.

Fine-tuning the graft parameters is a possible way to further unlock the potential of CNCs. Among various parameters, graft length is key to engineering the interface thickness and filler-matrix adhesion and, consequently, composite properties. Earlier studies have shown the

* Corresponding author at: Department of Material Science and Engineering, Clemson University, Clemson, SC 29632, United States.
E-mail address: spilla@clemson.edu (S. Pilla).

https://doi.org/10.1016/j.carbpol.2021.118405
Received 4 May 2021; Received in revised form 30 June 2021; Accepted 4 July 2021
Available online 10 July 2021

critical role of the graft length of poly(ε-caprolactone) (PCL) on the interfacial adhesion and toughening, suggesting a length threshold beyond which the PCL-PCL chain entanglement at the interface is continuously enhanced with an increase in PCL length (Nordgren et al., 2013). However, in the few studies that characterized graft lengths carefully, some seemingly contradictory results were presented. For example, when graft and matrix polymers are completely miscible (e.g., both were PCL), longer grafts resulted in higher strength and stiffness (Lönnberg et al., 2011). While for the less miscible pairs (e.g. poly(n-butyl methacrylate) (PBMA) graft and PLA matrix (Mamun et al., 2015)), better reinforcement was seen in shorter grafts (Boujemaoui et al., 2017). In both cases, not surprisingly, no toughening was observed due to the lack of a rubber domain. Consequently, the aforementioned discrepancies are possibly associated with graft-matrix miscibility as well as the range of graft length investigated. Previous studies clearly display the impacts of graft length on the composite properties and demonstrate the complexity in rational engineering of the CNC surface.

Tuning of graft length could be achieved by: (1) directly grafting the pre-synthesized polymers to the CNC surface ("grafting-to" method) or (2) synthesizing polymer from CNC surface and controlling the degree of polymerization by varying the content of monomer (Lönnberg et al., 2008), reaction period (Carlsson et al., 2015), or the content of sacrificial initiator (Boujemaoui et al., 2017) ("grafting-from" method). Though the "grafting-from" method yields higher graft density and molecular weight (Mw) due to less steric hindrance, the graft length is more difficult to control and has a relatively broader molecular weight distribution (Lönnberg et al., 2011). In addition, most reported studies adopted a method of ROP (Carlsson et al., 2015; Lönnberg et al., 2008) or atom transfer radical polymerization (ATRP) (Boujemaoui et al., 2017), in which only a few types of graft polymers (e.g., PCL, PLA, or PBMA) could be synthesized. On the other hand, the "grafting-to" strategy has larger latitude in choosing different types of grafts with precisely determined graft length. Among numerous conjugate chemistries applicable to CNC surface grafting (Ryu et al., 2018; Zheng & Pilla, 2020), a bio-inspired polydopamine (PDA)-mediated methodology has recently drew attention because of its ease of use in aqueous solutions, which is particularly suitable for CNC surface modification. In this method, the dopamine auto-polymerizes to form a PDA layer on the CNC surface, allowing secondary reactions with thiols and amino groups. This methodology has been used to graft thiol-containing castor oil (Shang et al., 2018) and diamine (Hu et al., 2019) onto CNC surfaces.

The present study aims to correlate graft length with the mechanical properties of nanocomposites. We select PEG and PVA as graft and matrix polymers because of the following considerations: (1) PEG-NH_2 of variable length are commercially available; (2) PEG-NH_2 is water-soluble, permitting the PEG-CNC grafting to be conducted effortlessly in water; (3) PEG and PVA are partially miscible, allowing the generation of robust CNC-matrix interactions (Falqi et al., 2018); (4) solvent casting mitigates the possible orientation of rod-like CNCs, avoiding the introduction of anisotropicity to complicate the interpretation of the mechanical results (Zheng & Pilla, 2020); (5) the unmodified CNC itself disperses well in the PVA matrix, thus any improvement in mechanical properties is likely due to the interfacial interaction rather than the enhanced dispersion caused by the PEG grafting. These considerations lead to the current design (using PEG grafts and PVA matrix) to elucidate the hypothesis that the variation of properties, if observed, is mainly due to the interfacial graft and graft length. On this platform, we purposefully designed a series of CNCs with PEG grafts of different lengths. PEG ($T_g = -20$ °C) forms a rubbery region surrounding the CNC rod. Amine-terminated PEGs (PEG-NH_2) of defined length, i.e., 1 k, 2 k, 5 k, and 10 kDa, were grafted to CNCs via the PDA-mediated method. Though the graft lengths chosen for this study are relatively shorter than other studies (Boujemaoui et al., 2017), the molecular diameters (approximate 2.3 to 9.1 nm according to Ref. (Cruje & Chithrani, 2014)) are comparable to the width of the CNCs. We expected that such a "thin rubbery layer" is beneficial in unlocking the reinforcing potential of CNCs. The poly(vinyl alcohol) (PVA)/CNC nanocomposites were prepared by solvent casting, with final CNC contents of 0, 1, 3, 5, 7 wt%. Simultaneous increases in stiffness and toughness were achieved by fine tuning the PEG graft length, which regulated CNC-matrix interfacial interactions.

2. Experimental

2.1. Materials

A 12.2 wt% aqueous dispersion of CNC was prepared by sulfuric acid hydrolysis at the USDA Forest Service, Forest Products Laboratory using previously established protocols (Reiner & Rudie, 2013). Dopamine hydrochloride (99%, Alfa Aesar), tris(hydroxymethyl) aminomethane (ACS certificated, Alfa Aesar), and polyvinyl alcohol (PVA, Sigma-Aldrich, 89–98 kDa, 99+% hydrolyzed) were commercial chemicals. Amine-terminated PEG (or PEG-NH_2 for accuracy) of different Mw (PS1-N-nK, $n = 1, 2, 5, 10$) were purchased from Ponsurebio Inc., China. Their molecular structure is CH_3-O-(CH_2-CH_2-O)$_n$-CH_2-CH_2-NH_2, where "n" is estimated to be 19, 40, 102, and 207, respectively.

2.2. Preparation of CNC-PEG

First, dopamine was polymerized to polydopamine (PDA) in solution and deposited on the CNC surface to form a PDA layer. Briefly, 50 mL buffer (0.01 M Tris-HCl, pH = 8.5) containing 0.1 g dopamine hydrochloride and 0.1 g CNC were magnetically stirred for 5 h at room temperature. During this process, the light blue opalescent solution turned black. Then, the obtained mixture was centrifuged at 5 k rpm for 5 min (Clinical 50, VWR) to precipitate the PDA-coated CNC (CNC-PDA). A portion of the supernatant was decanted, leaving approximately 8.5 mL of concentrated suspension in the centrifuge tube. Subsequently, another ~8.5 mL DI water with 0.1 g PEG-NH_2 was mixed with the above suspension followed by magnetic stirring overnight. The resultant PEG-grafted CNC (CNC-PEG) was collected and subjected to a thorough dialysis (cutoff 15,000 Da) against DI water for 10 days to remove the unbonded PEG. Finally, the CNC-PEG suspension was adjusted to 20 mL to yield a CNC concentration of 5 mg. CNCs grafted with different PEG lengths are abbreviated as CNC-PEGα, where α (α = 1 k, 2 k, 5 k, and 10 k) denotes the Mw (in Da) of the PEG-NH_2 used.

2.3. Solvent cast composite films

PVA containing 1%, 3%, 5%, and 7% of the unmodified and PEG-grafted CNCs were prepared by solvent casting. It is noted that, when denoting the concentration of CNC-PEG in the composites, it only considered the weight of CNC core, excluding the mass of PEG coating. Such method makes the measurement easy, especially suitable for the "never-dried" process from CNC to CNC-PEG, and to CNC-PEG/PVA solution. Briefly, a 4% PVA solution was prepared by dissolving PVA powder in the DI water followed by refluxing at 90°C for 4 h. After cooling to room temperature, the PVA solution was mixed with the unmodified CNC or CNC-PEG suspension by magnetic stirring, cast into a glass mold, and then dried under ambient conditions (25 °C) for 7 days. The films were then removed from the mold and conditioned in a fume hood for another 10 days. The process schematic can be found in Fig. 1.

2.4. Characterization

The morphology of the CNCs was determined by Transmission Electron Microscope (TEM, Hitachi H7600) operated at an 80-kV accelerating voltage. The specimens were prepared by applying a drop of dilute CNC suspension (~0.025 mg/mL) on a silicon oxide coated grid followed by the uranyl acetate staining. The chemical compositions of CNCs and composites were characterized by Attenuated Total

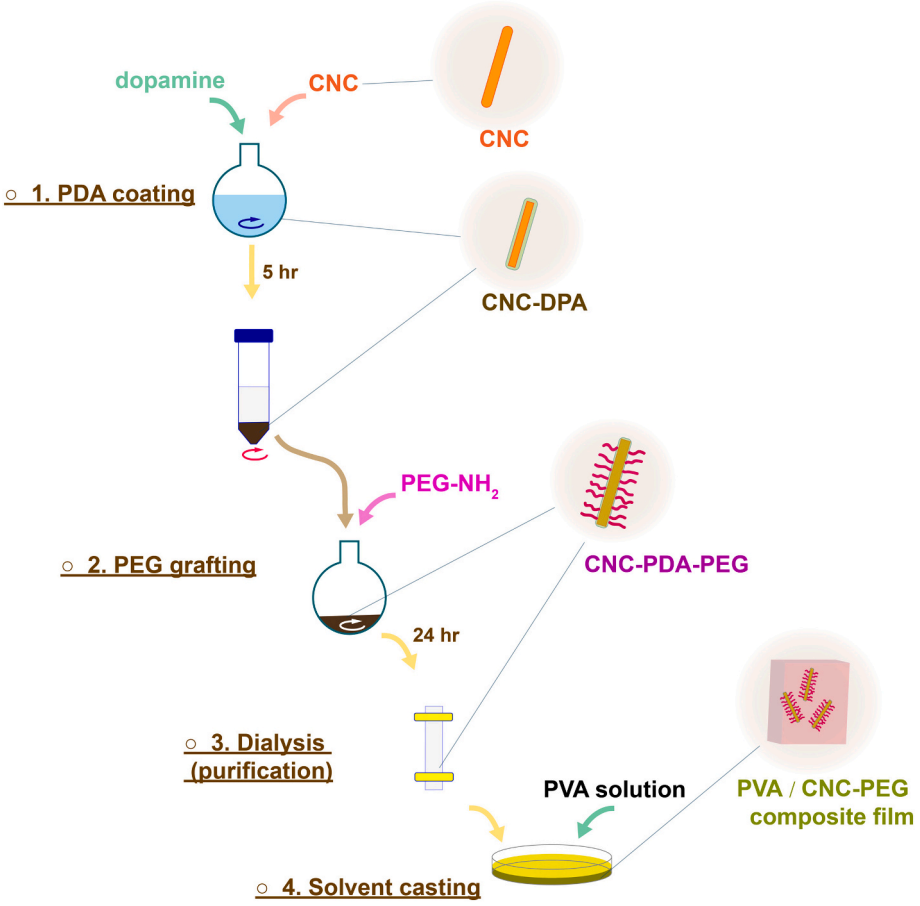

Fig. 1. PVA/CNC-PEG preparation.

Reflectance Fourier Transform Infrared (ATR-FTIR, Thermo-Nicolet Magna 550) spectroscopy. Absorption spectra were recorded for wavelengths from 4000 to 500 cm^{-1} with a resolution of 2 cm^{-1}. The surface compositions of CNC-PEGs were characterized by X-ray photoelectron spectroscopy (XPS, Physical Electronics, USA). A VersaProbe III spectrometer was used with a monochromatic Al X-ray source operating at 15 kV and 25 W, with a beam spot diameter of ~100 μm. Deconvolution of C 1s and N 1s were conducted. N 1s curves were subjected to smoothing by adjacent averaging before the deconvolution. The ζ potential and particle size (hydrodynamic diameter) were measured by a Zetasizer Nano ZS90 analyzer (Malvern instrument, Worcestershire, UK). The dialyzed CNCs were diluted to 0.025 mg/mL with DI water and measured at 25 °C. Values were averaged over three tests. The thermal behaviors of the composite films were analyzed using a differential scanning calorimeter (DSC, Q200, TA Instrument). Samples were subjected to sequential heating-cooling-heating scans between 40 °C and 240 °C at a rate of 5 °C/min. The thermogravimetric assays (TGA, Q5000, TA instrument) were analyzed from 25 to 900 °C at 10 °C/min in N_2. Both temperature ramps and isothermal strain sweeps were performed in tensile mode on a TA Q800 dynamic thermomechanical analyzer (DMA). Films (0.096–0.152 mm in thickness) were trimmed to strips of ~5 mm in width and grip distance was set at 12−15 mm. After mounting, the temperature was first increased to 130 °C and then cooled to 0 °C to remove any residual moisture. Temperature ramps were conducted at a frequency of 5 Hz and a strain amplitude of 5 μm from 0 to 200 °C at 3 °C/min. Isothermal strain sweeps (4 replicates) were conducted at a fixed frequency of 1 Hz at both 25 °C and 80 °C until the maximum drive force (35 N) was reached. Tensile properties including elastic modulus, yield strength, ultimate strength (US), strain at break (ε), and toughness (as determined by the area under the strain-stress curve), were measured using an Instron Universal testing machine (Model 1125) at cross-head speed of 10 mm/min with a 31 mm grip separation as per ASTM D882-12. Rectangular tensile specimens were 10 mm wide and the thickness was measured by a film thickness gauge. Prior to testing, specimens were conditioned at 23 °C and RH = 55% for 10 days.

3. Results and discussions

3.1. Polydopamine-mediated PEG grafting

The PEG grafting is based on a bioinspired catechol chemistry. Although there is no consensus on the mechanism of PDA coating, it is believed that oxidation of dopamine by dissolved oxygen triggers the formation of a series of oxidation products, e.g., the dopamine-quinone and 5,6-dihydroxyindole (DHI), and further form other higher molecule species through covalent interaction or self-assembly (Ryu et al., 2018). These molecules are of low solubility and deposit on the substrate surface to form a PDA conformal coating through covalent interaction, hydrogen bonding, π-π interaction, and other interactions. Such PDA-modified surfaces are reactive toward primary amine groups through the Schiff-base reaction or Michael addition (Ryu et al., 2018), which is the basis of the PEG grafting, as illustrated in Fig. 2a.

For the purpose of surface activation, a thin and uniform PDA layer is imperative. The extent of PDA treatment can be easily adjusted by varying the dopamine treatment time (Ryu et al., 2018). Short PDA treatment times (e.g., <4.5 h) retain CNC's exceptional electrostatic stability, creating difficulties in separating CNC by centrifuging, whereas long PDA treatment times (e.g., >10 h) lead to flocculent agglomeration and poorly defined CNC surfaces (Fig. 2b). CNC-PDAs

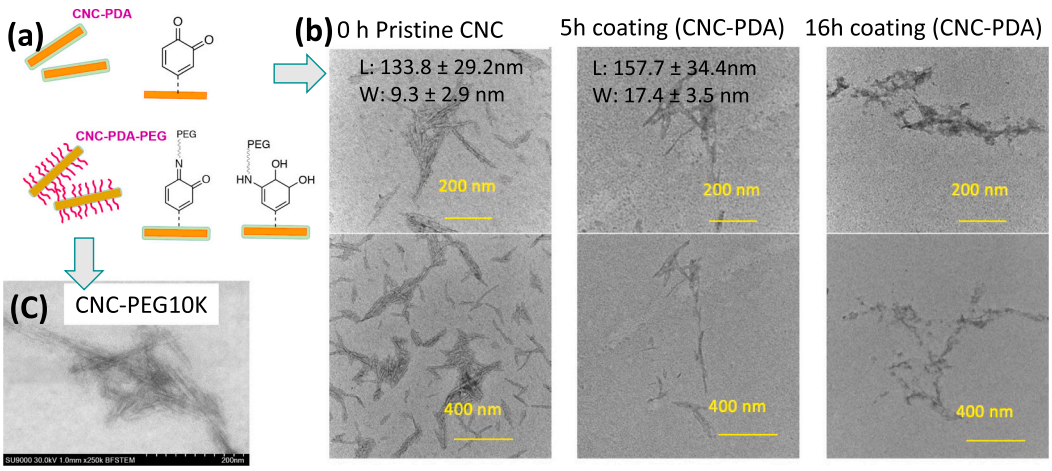

Fig. 2. (a) Suggested chemistry of PDA surface modification (top) and PEG grafting (bottom). (b) TEM images of pristine CNC and PDA treated CNC for 5 h and 16 h. (c) TEM image of CNC-PEG10kk.

treated for 5 h resulted in a thin PDA layer (4–6 nm), a clear CNC contour, good CNC dispersity, and easy separation by centrifuging.

Though TEM imaging reveals the evolution of the morphology upon the PDA treatment, suggesting amine-terminated PEG was bonded to the PDA-activated CNC surface (Fig. 2c), characterizing the PEG grafts (e.g., the grafting density) is challenging. The absolute PEG graft content is difficult to measure gravimetrically, due to the possible CNC loss during multiple centrifuging. Also, the similar elemental composition of CNC and PEG (C, H, N, and O) doesn't allow methods, such as elemental analysis (Ohno et al., 2005) or selective etching (Zhou & Huck, 2006), to distinguish PEG from CNC. Eventhough, the addition of PEG is considered to be in excess. The molecular diameter of the PEG is estimated to be 2.3, 3.5, 6.0, and 9.1 nm (for 1, 2, 5, 10 kDa) in water (Cruje & Chithrani, 2014). The amount of PEG is hundreds-folded higher than necessary to create a PEG monolayer (see Supporting Information) and high grafting would result in the brush conformation.

In addition, confirming the PDA coverage is essential. The PEG molecule itself has inherent affinity toward CNC's unmodified surface (Pereda et al., 2014). If much of the original CNC surface remains exposed, it will weaken the hypothesis regarding the PDA-induced PEG grafting. The level of PDA coating was evaluated by FTIR and XPS. The FTIR spectra of CNC-PDA exhibits features inherent to the CNC core and the PDA coating, while the CNC-PEG spectrum is a trio of CNC, PDA, and PEG. Given that the penetration depth of IR (typically 0.5–5 μm (Schuttlefield & Grassian, 2008) exceeds the dimensions of the PDA-CNC, IR merely reflects the overall composition of the PDA-CNC (see Table S1 and Fig. 3a for FTIR bands assignment). On the other hand, with a penetration depth of only 8–10 nm, XPS is more of a surface analysis technique. The angle-resolved XPS (45°) used in this study further enhances the contribution from the surface. The surface atomic elemental percentages of S (S%) and N (N%) determined by XPS are shown in Fig. 3b. S% is an indicator of the original CNC surface, because sulfur was introduced during the sulfuric acid hydrolysis for the CNCs preparation, while N% is relevant to the PDA and PEG coatings. S% of the pristine CNC decreased from 0.62% to 0.51% after PDA coating (5 h), and then varied slightly from 0.44%, 0.49%, 0.53% after grafting PEG of 1 k, 2 k, and 5 k, respectively (Fig. 3b). A notable S% reduction was observed after the PEG10k grafting (S% = 0.22%), because the signals exponentially attenuated with increase in coating thickness (DPA layer plus PEG layer). N%, on the other hand, displayed a more complicated trend; thus 3 spots were measured to confirm the results. The monotonic increase of N% from 0 h, 5 h to 24 h of PDA coating confirms the PDA thickening over the incubation time, while the monotonic decrease of N%, from CNC-PEG2k, −5 k, to −10 k, can be attributed to the reduced proportion of nitrogen endcap along with the

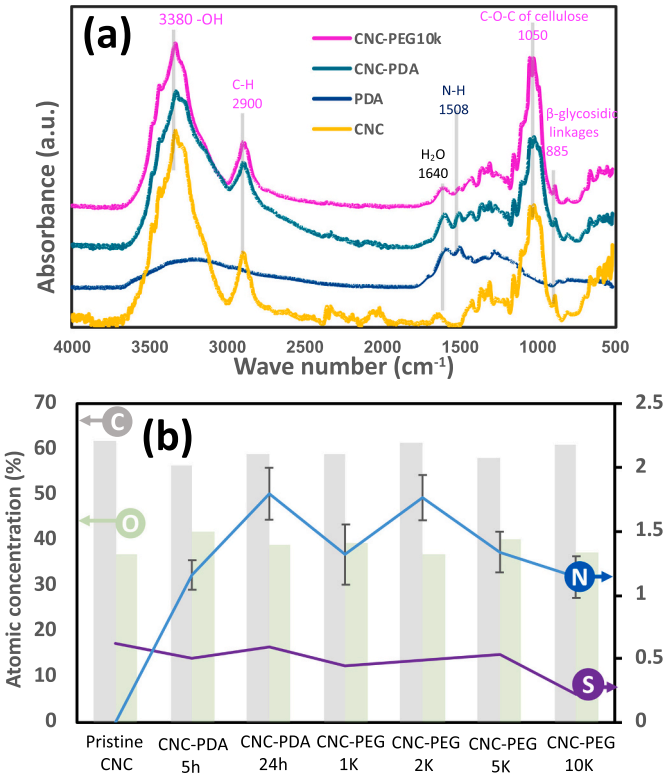

Fig. 3. (a) FTIR and (b) atomic percentage of CNC particles.

increase in PEG's molecular weight. The N% of CNC-PEG (average of 1.8%, 1.3% and 1.1% for 2 k, 5 k and 10 k PEG ligands) are ~1% higher than the theoretical N% of their corresponding PEG-NH_2 (0.8%, 0.3%, and 0.2%) probably because of the N contribution of the PDA layer underneath. Fig. S1 shows the deconvolution spectra of N s1 corresponding to 3 components, i.e., R—NH_2 (N1, 401.8 eV), R_1—NH—R_2 (N2, 399.9 eV) and C═N—R (N3, 398.6 eV) (Feng et al., 2016). The N1:N2:N3 ratio is summarized in Table S2. N1 (R—NH_2) is mainly from the dopamine monomer and PEG-NH_2, while N2 (R_1—NH—R_2) and N3 (C═N—R) are from the 5-6-dihydroxyindole (DHI)-related features and the PEG-PDA linkage (Feng et al., 2016). Interestingly, the proportion of N1 seems decreased over the increase of PEG length, probably implying that the consumption of R—NH_2 (N1) accompanied the formation of R_1—NH—R_2 (N2) in the reaction between PDA and PEG-NH2 (Table S2).

This result further supports the occurrence of a grafting reaction rather than the PEG physical adsorption.

Fig. 4 shows the effects of the PEG grafting on the electrical charge environment and the hydrodynamic diameter of the CNC particles. The pristine CNC exhibited a negative zeta potential ($\xi^d = -41.8$ mV) in DI water (pH = 6.5) because of the surface sulfate esters introduced during the H_2SO_4 hydrolysis. Such a negatively charged surface contributes to the electrostatic stability of the CNC suspension. Surprisingly, PDA shielding increased the charge density slightly ($\xi^d = -46.1$ mV), which is consistent with some reports (Han et al., 2016), but conflicts with others (e.g., $\xi^d = -15$ mV (Fu et al., 2015). Such discrepancies might be associated with the variation in coating thicknesses in different studies. PEG grafting slightly decreased the overall charge, from −48 mV for CNC-PDA to −35 mV for CNC-PEG10K. The monotonic increase of ξ^d over the PEG length implies a better shielding efficiency of the long grafts. The long PEG grafts formed a thicker PEG layer, resulting in the surface of the hydrodynamic sphere being farther from the negatively charged CNC core. Though the charge density was reduced, CNC-PEG couldn't be precipitated by centrifuge after PEG grafting due to the steric repulsion of the PEG layer. The interpretation of the parameter of *Z*-average size is slightly tricky for the rod-shaped CNCs since DLS measures the hydrodynamic diameter (D_h), which is more definable for a spherical geometry. DLS gave a Z-average size of 75 nm for the pristine CNCs (Fig. 4), which is comparable to other reports (Azzam et al., 2010). The D_h increased monotonically with the graft length, supporting the dimensional increase with PEG graft length.

3.2. Properties of composite films

To study the PEG graft length effects on the properties of composites, PVA/CNC films were prepared by solvent casting. Since the mechanical properties of PVA films are susceptible to moisture (Konidari et al., 2011), specimen were conditioned at 23 °C and RH = 55% for 10 days prior tensile testing.

It is possible that PEG grafting has effects on the mechanical properties of the composites and that all are closely related to matrix-filler interaction and interface morphology. The thermal behavior, degree of crystallization, and moisture contents are presented in Table 1. The crystallization temperature (T_c) reveals how the PEG graft influences the PVA crystallization at the interface. The addition of CNC (e.g., 5%) promoted crystallization through nucleation, resulting in higher crystallinity (χ_c%, from 30.9% to 43.4%) and an increased T_c (from 205.0 °C to 209.6 °C). The surface PEG grafting, however, inhibited this process somewhat and lowered the T_c slightly at high graft length (Fig. 5a). Admittedly, without knowing the graft density among the CNC-PEGs, correlating property change to PEG length is challenging. However, the change in the T_c provides a direct indication of the filler-matrix interaction via molecular entanglement (assuming the area of the interfaces are comparable), which is closely related to the graft length.

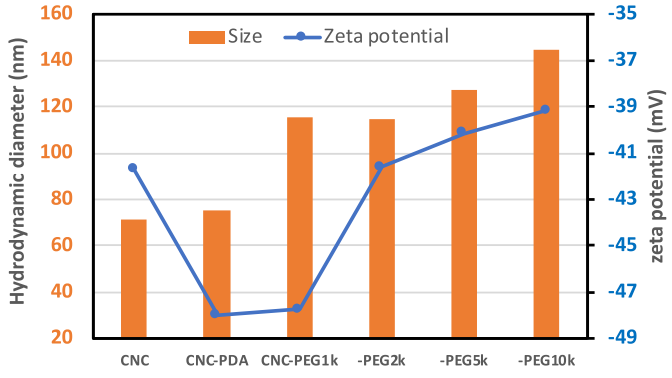

Fig. 4. Hydrodynamic diameter and zeta potential of CNC particles.

Impacts of PEG length on the thermal stability of films were also evident (Fig. 5b). Adding CNCs to PVA significantly delayed decomposition perhaps due to the increased crystallinity induced by the CNCs (Table 1). The grafting of PEG onto the CNC surface further increased thermal stability, especially with shorter PEG grafts. The derivative TGA curves (Fig. 5b) suggest a two-stage-degradation of PVA: 1) the dehydration of hydroxyl groups at low temperature (250–350 °C) followed by 2) the chain-scission at high temperature (above 350 °C) (Peng & Kong, 2007). Minor discrepancies in the temperature ranges appearing in the literature is perhaps due to the different hydrolysis degrees of PVA. Zheng et al. hypothesized that reagents that prevent the formation of protonated hydroxyl groups of PVA could suppress its dehydration (the first stage) (Peng & Kong, 2007). In our case, the primary and secondary amine-rich PDA layer is more nucleophilic than the hydroxyls on the pristine CNC surfaces, competing with the protonation of CNC hydroxyls to create the leaving group, —OH^+, for the dehydration. If this is the case, short PEG grafts may expose more accessible amines (PDA layer) that suppress PVA dehydration, while long PEG graft may have larger coverage, isolating the PDA layer from the PVA. It is worth noting that data of CNC-PDA filled film is not presented in the above discussion, which could serve as a useful control in elucidating the hypothesis of amine-suppressed dehydration. This is because CNC-PDA particles showed agglomerates in the process of water evaporation to form composite films, resulting in poor repeatability in results of TGA, tensile, and dynamic thermal-mechanical analysis.

3.3. Effects of graft length on the mechanical properties of composite films

The tensile strengths of the PVA films are shown in Fig. 6a. The expected CNC reinforcement was not clearly seen with unmodified CNC (red dash frame) and the tensile strength even decreased upon low CNC addition (1% and 3%), although it slightly increased at high CNC loading (5% and 7%). A possible reason for this is the increase in moisture content with the addition of CNC, leading to increased ductility as a result of plasticization by the water. The moisture content determined by the weight reduction below 130 °C from the TGA curves (green frame in Fig. 5b, Table 1) confirmed the higher moisture content in the PVA/CNC (7.4–8.9%) relative to the pure PVA (6.8%). Interestingly, regardless of PEG length, films filled with PEG-grafted CNC showed less variation in moisture content (from 6.9% to 7.2%, for 5% filler loading, see Table 1). Thus, moisture content should not be considered a primary influence when comparing the mechanical properties of composites containing CNCs of different graft length.

For composites filled with CNC-PEGs, a typical increasing trend in ultimate strength (US) with reinforcing filler loading was observed for films with CNC-PEG2k (blue frame in Fig. 6a, Fig. S2) but not for those with CNCs with 1 k, 5 k and 10 k grafts. Such inconsistencies make drawing conclusions regarding the effect of graft length on US difficult. However, the CNC-PEGs did generally demonstrate greater reinforcement than the unmodified CNCs, increasing US by 9%–47% at optimal graft lengths for each CNC loading.

Unlike US, the length-effects on the other tensile properties are somewhat clearer. For the unmodified CNCs (black frame in Fig. 6b), the stiffness of composites changed little until the CNC loading exceeded 5%. This increase could be a sign of the formation of a percolated network of stiff CNCs (Zheng & Pilla, 2020). Interestingly, such a threshold was not evident for PEG-grafted fillers. Instead, the stiffness increased more consistently with filler loading (green frame in Fig. 6b). This could suggest that the PEG grafting decreases the percolation threshold due to the PEG-PEG interaction and facilitates the formation of percolation networks. In addition, shorter grafts generally yielded higher moduli, regardless of the filler loading. While somewhat variable, the elongation at break (ε) increased considerably with PEG grafting, leading to higher toughness as well (Fig. 6c–d). The highest ε and toughness appeared more frequently at a moderate PEG length (i.e., 5 k), while the lower CNC-PEG content, e.g., 1%, was favorable for high ε and

Table 1
Thermal properties and moisture content of films.

Filler type	Filler content (CNC basis)	T_g (°C)[a]	T_m (°C)[b]	ΔH_m (J/g)[b]	χ_c%[c]	T_c (°C)	Moisture content[d]
None (neat PVA)	0	75.4	227.4	48.16	30.9%	205.0	6.8%
CNC	1%	76.4	229.5	70.44	45.6%	211.0	7.4%
CNC	3%	77.8	225.9	70.57	46.6%	211.2	7.6%
CNC	5%	78.3	226.3	64.34	43.4%	209.6	7.5%
CNC	7%	80.1	227.0	63.62	44.1%	209.2	8.9%
CNC-PEG1k	5%	79.8	225.8	67.61	45.6%	209.2	7.0%
CNC-PEG2k	5%	79.5	225.4	63.57	42.9%	209.4	7.2%
CNC-PEG5k	5%	79.6	225.7	64.21	43.3%	209.2	7.2%
CNC-PEG10k	5%	79.6	225.8	63.49	42.8%	208.9	6.9%

[a] Glass transition temperature (T_g) was obtained from the 2nd heating cycle.
[b] Melting temperature (T_m) and melting enthalpy (ΔH_m) was obtained from the 1st heating cycle.
[c] $\chi_c = \Delta H_m/\Delta H_m^0 \times 100/a$ where $\Delta H_m^0 = 156$ J/g the ΔH_m of 100% crystalline and a is the weight fraction of the plastic. Here a is approximated to be 1- CNC% (neglecting the portion of PDA and PEG), for simplicity.
[d] Measured by TGA.

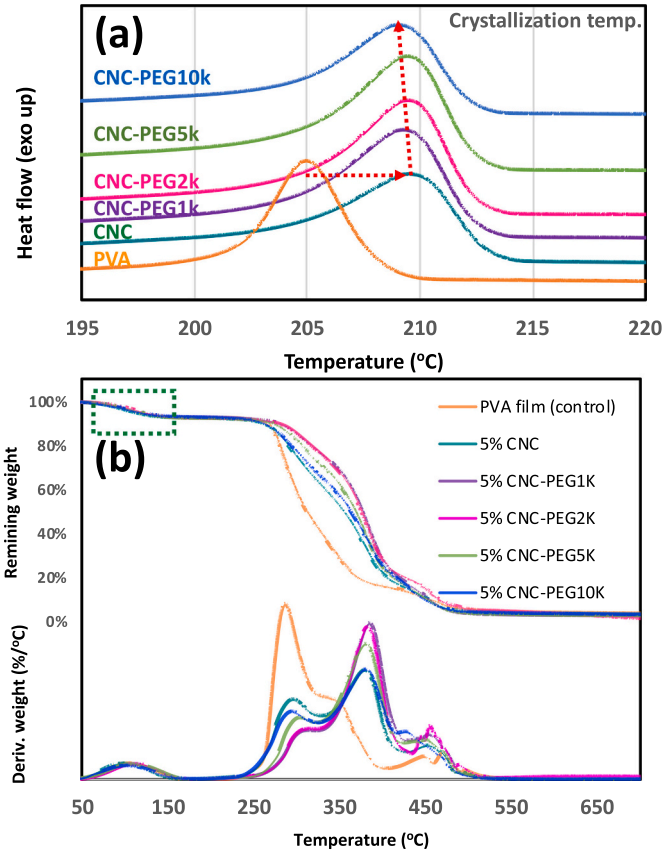

Fig. 5. (a) Tc of films and TGA curves (b) of PVA films at 5% filler loading.

toughness. The higher ε and toughness are not likely caused by the plasticizing effects of free PEG because of (1) a dialysis process used to eliminate the unbonded PEG; (2) the lack of evidence supporting the existence of free PEG in composites (e.g., lowering of the T_g or increased XPS intensity at 401.8 eV in Fig. S1 associated with a large quantity of free —NH_2); and (3) the fact that higher filler loading, and concomitant higher free PEG content, did not result in higher ductility (Fig. 6c–d). This suggests that it is the PEG graft length affecting the mechanical properties.

Though T_c and TGA reveal some length effects on composites properties, they probe the interfacial conditions in indirect ways. The PEG grafts play their roles when force is applied, thus the dynamic mechanical behavior of the interface is more pertinent to understanding the effects of graft length on mechanical properties. Therefore, DMA analysis was performed on the films and an adhesion factor (A^*) was derived to analyze the filler-matrix interface. If the loss factor (tan δ_c) for a particle-filled composite is assumed to be the sum of the contributions of the filler (subscript *f*), interface (*i*), and matrix (*m*), then:

$$tan\delta_c = v_f tan\delta_f + v_i tan\delta_i + v_m tan\delta_m, \quad (1)$$

where v is the volume fraction of each component. Assuming $\tan\delta_f \cong 0$ and v_i is small, Eq. (1) simplifies to:

$$tan\delta_c / tan\delta_m \cong (1 - v_f)\bullet(1 + A^*), \quad (2)$$

where,

$$A^* = \left[v_i/(1 - v_f)\right]\bullet(\tan\delta_i/\tan\delta_m) \quad (3)$$

Rearranging Eq. (2) yields:

$$A^* = \left[1/(1 - v_f)\right]\bullet(\tan\delta_c/\tan\delta_m) - 1. \quad (4)$$

A^* is clearly proportional to the interfacial contribution (i.e., $v_i \times \tan\delta_i$) (Eq. (3)) and can be expressed by the measurable parameters: $\tan\delta_c$, $\tan\delta_m$ and v_f (Eq. (4)). The higher the interfacial adhesion, the lower the contribution of the interface to damping and the lower the value of A^*. More details of A^* can be found in Kubat et al. (1990). Table 2 and Fig. S3 present the values for tan δ_c and A^* for our composite films. Films with CNC-PEGs have lower values of A^* than those with untreated CNCs, suggesting that PEG grafting enhanced interfacial adhesion and reduced its contribution to the overall damping. Notably, long PEG grafts do not necessarily lead to better interfacial adhesion (i.e. lowest A^*) than short ones, despite increased PVA-PEG entanglement (Fig. 6a). A possible reason is interface slippage associated with the interface thickness, as detailed below.

Composite damping is caused by filler-matrix interfacial friction. The strain-dependence of damping has been observed and interpreted by the "stick-slip" mechanism (Suhr & Koratkar, 2008). At small strains, stress is transferred across the filler-matrix interface to the more rigid filler, contributing to the overall composite modulus. At a critical stress, the interface debonds and slips, while the stress that the filler bears remains at its maximum. Such relative displacement at the interface causes the friction and energy dissipation (Suhr & Koratkar, 2008). The stick-slip transition results in a slight reduction in the storage modulus (right side of the dashed line in Fig. 7a) and an increase of the loss modulus (energy dissipation). The plateau of the loss modulus suggests that the majority of the slippage has been activated (Fig. 7b) (Suhr & Koratkar, 2008). To confirm this stick-slip mechanism, Suhr et al. prevented interfacial slippage by introducing a rigid chain covalently bridging single-walled carbon nanotubes (SWCNT) and a polycarbonate matrix (Suhr & Koratkar, 2006). Higher storage modulus and lower loss modulus were observed over the strain from 0.2–1.2% compared to its unmodified SWCNT counterpart. These results were interpreted as the

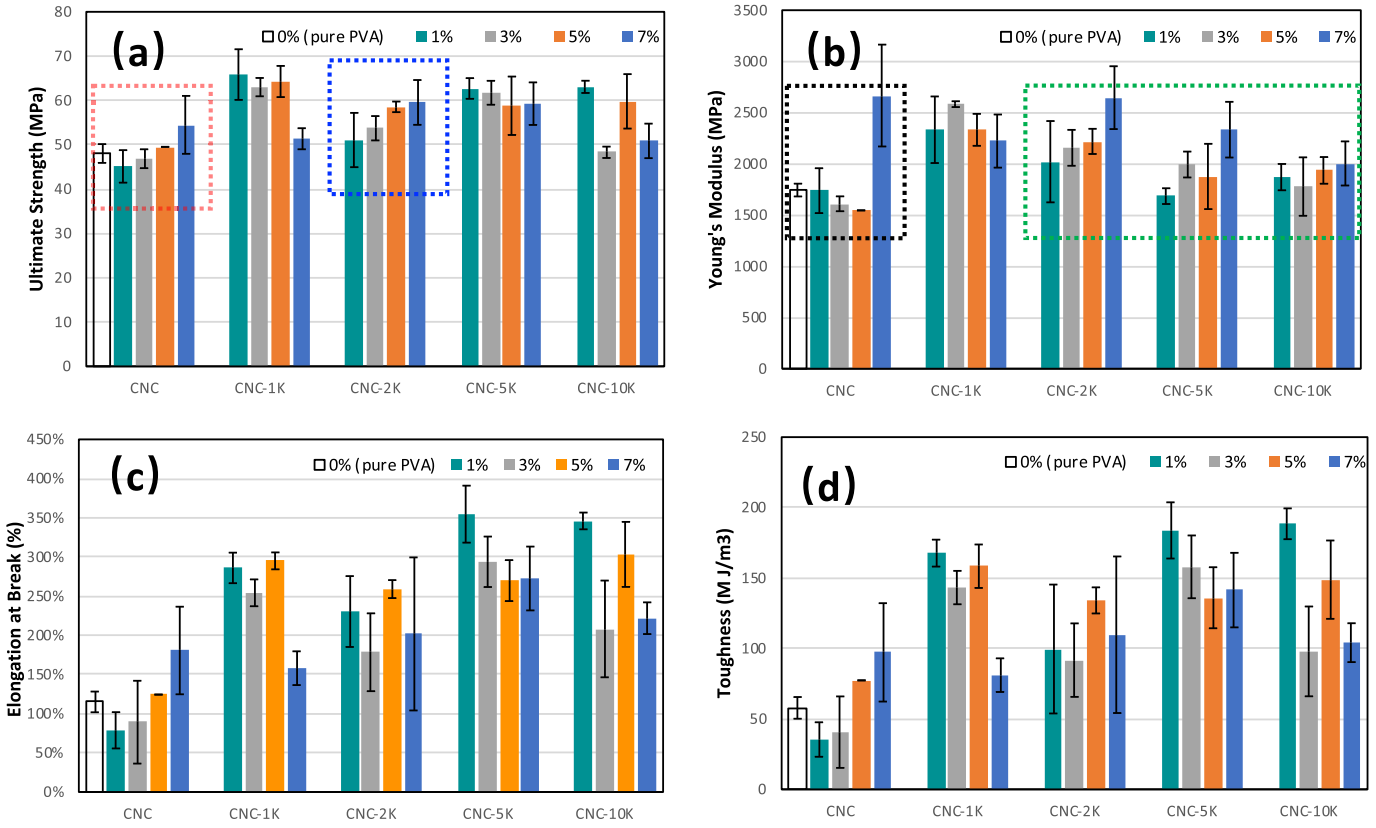

Fig. 6. Mechanical properties of nanocomposite films: (a) ultimate strength, (b) Young's modulus, (c) strain at break, and (d) toughness.

Table 2
Loss factors (tan) and adhesion factors (A^*) values for PVA/CNC composites.

Filler type	tan $\delta_{c,}$ 30°C	$A^*_{30°C}$	tan $\delta_{c,}$ 50°C	$A^*_{50°C}$	tan $\delta_{c,}$ 80°C	$A^*_{80°C}$
Pure PVA	0.038	–	0.044	–	0.105	–
CNC	0.037	0.016	0.045	0.052	0.094	−0.052
CNC-PEG1k	0.028	−0.226	0.035	−0.180	0.082	−0.173
CNC-PEG2k	0.037	0.003	0.044	0.027	0.088	−0.117
CNC-PEG5k	0.028	−0.238	0.034	−0.194	0.083	−0.169
CNC-PEG10k	0.034	−0.078	0.041	−0.058	0.090	−0.098

covalent interfacial bonding facilitating stress transfer and increasing stiffness, while preventing the slippage that would lead to energy dissipation.

Our study adds further perspective on the stick-slip mechanism by investigating the effects of an interface of variable thickness (as controlled by graft chain length) and comprised of a soft polymer with one free end. Films containing CNC-PEG with longer surface grafts required larger strains than shorter grafts to maximize stress transfer and to transition to a slip mechanism (Fig. 7a–b). However, films with long grafts exhibited low storage modulus in the plateau region (Fig. 7a), suggesting low stress transfer efficiency. This helps explain the lower stiffnesses in tensile tests of films with higher graft lengths (e.g., orange columns in Fig. 6b). We hypothesize that the PEG interfacial layer contains three domains, the bonding domain, the PEG domain, and the anchor domain, as illustrated in Fig. 7e. The anchor domain governs the matrix-filler stress transfer, while the PEG domain contributes to the damping behavior. Shorter grafts are expected to lead to higher graft density than long grafts and thus more interaction sites (i.e., anchors) are available to interact with matrix polymer chains, resulting in the higher stress transfer efficiency and higher stiffness. On the contrary, though long grafts have large CNC surface coverage and better entanglement with the matrix polymer (as evidenced by the TGA and DSC results), the graft density is likely lower due to steric hindrance. Thus, fewer anchor sites exist and less stress transfer pathways are available. As a result, lower stiffness is observed (Fig. 7). To further understand the role of the anchor region, the DMA measurements were conducted at elevated temperature (80 °C) aiming to deactivate the non-covalent PVA-PEG interaction above the melting point of PEG. The ungrafted CNC-filled film at the same filler loading (3%) was also measured, providing a control with a different type of interfacial interaction. As shown in Fig. 7c–d, E′ and E″ decreased at high temperature. Though the main reason for the loss of stiffness is the softening of the PVA matrix, both E′ and E″ of the CNC-PEG-filled films decreased more rapidly than their ungrafted CNC-filled counterpart (red hollow circle), implying that the factors that mediated the stress transfer at low temperature are diminished. In this study, we attributed this factor to the PVA−PEG interaction in the anchor region, which is absent in the PVA−CNC interface. In addition, the length-dependency of stick-slip transition in the curves for E′ and E″ are less discernible at high temperature (dash line in Fig. 7c–d), further supporting that the anchoring was deactivated.

Another aspect of the hypothesis relates to the role of the PEG layer on damping. PEG molecules have low interchain entanglement and low intermolecular forces, exhibiting mainly Newtonian behavior in its melt state. This was demonstrated by rheological measurement (Fig. S4) using PEG 10,000 as a model polymer, in which the viscosity of PEG melt was found to be independent of shear rate. Therefore, the PEG layer in our composite films could serve as an interfacial "lubricant", reducing friction under sinusoidal stress. Thick PEG layers led to the lower friction, reduced damping, and lower loss moduli (Fig. 7a and b). This also explains the lower adhesion factor (A^*) of the films with CNC-PEGs of long graft length (Table 2).

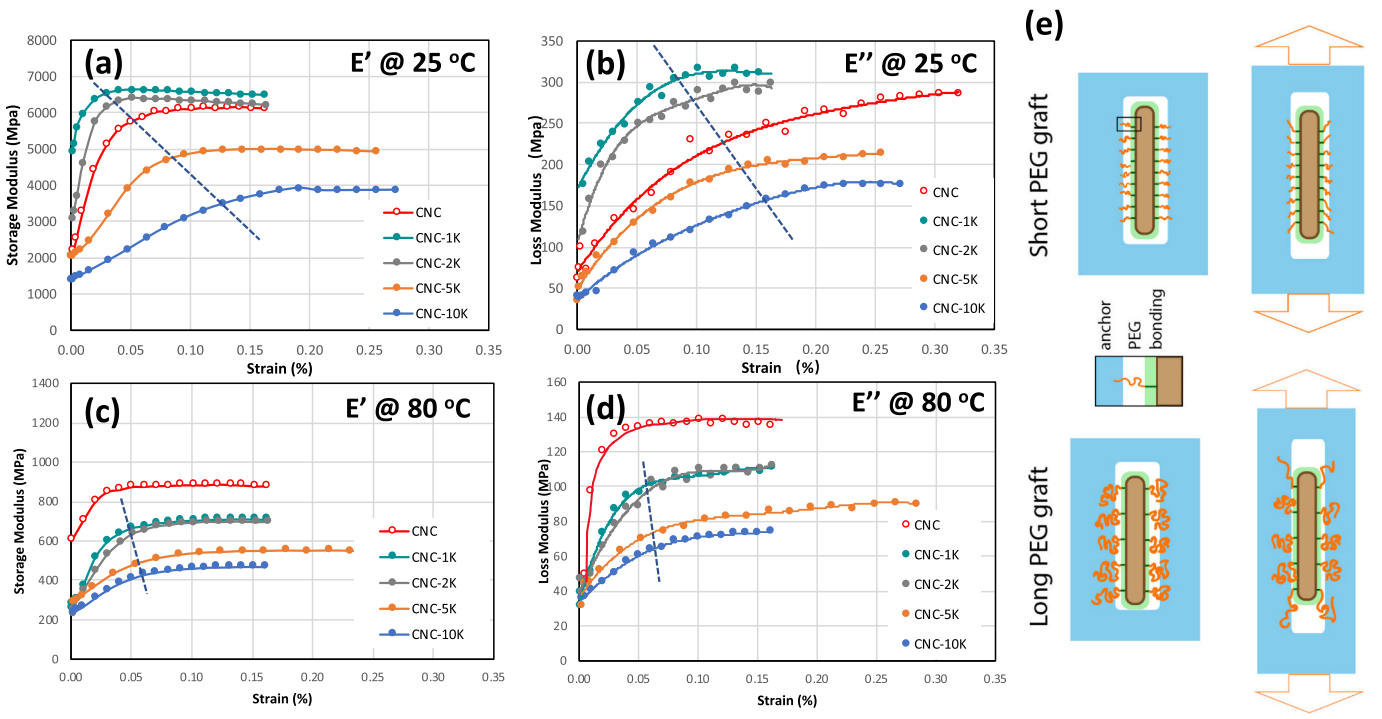

Fig. 7. Storage modulus conducted at 25 °C and 80 °C (a and c) and loss modulus conducted at 25 °C and 80 °C (b and d) as a function of dynamic strain amplitude for PVA film with 3% CNC of different PEG grafts. Schematic illustration of fillers under tensile strain (e).

The proposed model in Fig. 7e also helps explain the PEG-induced toughening observed in Fig. 6d. PEG is in its rubbery state at ambient temperature and may function like the rubber particles in many rubber-toughened plastics (Nagarajan et al., 2016). The long graft length (e.g., PEG5k) is associated with thick coating and high entanglement (Figs. 6b and 7e), all of which facilitates ductile behavior and results in toughening. Tensile toughening measures the ability to absorb energy during stretching, which are affected by toughening mechanisms such as shear yielding, crazing, and cavitation (Nagarajan et al., 2016). PEG length had little effect on yielding (Fig. S2), but significantly influenced elongation at break (Fig. 6c). The crazing-prone PVA specimens turned cloudy during the stretching, suggesting the formation of microvoids and fibrils that span the new surfaces prior to fracture. In this energy-absorbing process, the highly stretchable PEG grafts could serve as fibril bridges and carry the applied stress even at high strain. Cavitation may also contribute to toughening. The coating region of long PEG grafts is occupied by coiled PEG molecules with less PEG-PEG intermolecular interaction than that of the short PEG grafts. This region may deform first and induce internal cavitation which absorbs energy due to negative dilatational effects (Muiruri et al., 2019), and reduces constraints that limit yielding at crack tips.

Although many insights into the relationship between PEG graft length and mechanical performance were found, greater understanding was limited by the inability to quantify graft density. Methods including the ^{1}H NMR (Lönnberg et al., 2011) and solid-state NMR (King et al., 2018; Yoo & Youngblood, 2016) were attempted but were unsuccessful in the present study. More works are expected to provide further insight.

4. Conclusions

In summary, we have engineered the CNC with the PEG grafts of various lengths through a bioinspired catechol chemistry. These fillers were used to prepare PVA composite films by the solvent casting. The tensile strength, stiffness, and the toughness of the composite films were improved simultaneously (comparing to unmodified CNC-filled PVA). CNC with shorter grafts, e.g., CNC-PEG1k, exhibited improved stiffness and strength. Adding 1% CNC-PEG1k as a reinforcing filler, increased the ultimate strength and the stiffness of the composite 40.4% and 34.2% over its ungrafted counterpart. Pronounced enhancement in the toughness was observed when utilizing the CNC-PEG. For example, adding 1% CNC-PEG1k and 1% CNC-5 k improved the toughness of PVA by 150% and 220%, respectively. The enhanced mechanical properties were attributed to the filler-matrix interface, which depended on the PEG graft length. Long PEG grafts had higher PEG coverage, more intensive chain entanglement, and thicker PEG layers than short grafts. This resulted in lower interfacial adhesion and lower stress-transfer efficiency. On the other hand, the short PEG length strengthened PVA/CNC composites due to the high stress-transfer efficiency likely due to the high interfacial interaction.

CRediT authorship contribution statement

Ting Zheng: Investigation, Methodology, Formal analysis, Writing – original draft. **Craig M. Clemons:** Conceptualization, Methodology, Writing – review & editing. **Srikanth Pilla:** Conceptualization, Methodology, Writing – review & editing, Supervision.

Declaration of competing interest

The authors report no declaration of interest.

Acknowledgement

This work was support by the USDA National Institute of Food and Agriculture, AFRI project [contract number: 2016-67021-25016], the US Endowment for Forestry and Communities [grant number: E17-18], the Robert Patrick Jenkins Professorship, and the Dean's Faculty Fellow Professorship. T.Z would like to acknowledge partial financial support provided by Cooper-Standard Postdoctoral Fellowship. The authors are grateful to Limberly Ivey for her valuable suggestion and measurement on the DMA analysis, and Dr. Thompson Mefford and Zichun Yan for their assistance in the DLS measurement.

Appendix A. Supplementary data

Supplementary data to this article can be found online at https://doi.org/10.1016/j.carbpol.2021.118405.

References

Azzam, F., Heux, L., Putaux, J.-L., & Jean, B. (2010). Preparation by grafting onto, characterization, and properties of thermally responsive polymer-decorated cellulose nanocrystals. *Biomacromolecules, 11*(12), 3652–3659.

Boujemaoui, A., Cobo Sanchez, C., Engström, J., Bruce, C., Fogelström, L., Carlmark, A., & Malmström, E. (2017). Polycaprolactone nanocomposites reinforced with cellulose nanocrystals surface-modified via covalent grafting or physisorption: A comparative study. *ACS Applied Materials & Interfaces, 9*(40), 35305–35318.

Carlsson, L., Ingverud, T., Blomberg, H., Carlmark, A., Larsson, P. T., & Malmström, E. (2015). Surface characteristics of cellulose nanoparticles grafted by surface-initiated ring-opening polymerization of ε-caprolactone. *Cellulose, 22*(2), 1063–1074.

Cruje, C., & Chithrani, D. (2014). Polyethylene glycol density and length affects nanoparticle uptake by cancer cells. *Journal of Nanomedicine Research, 1*(00006).

Falqi, F. H., Bin-Dahman, O. A., Hussain, M., & Al-Harthi, M. A. (2018). Preparation of miscible PVA/PEG blends and effect of graphene concentration on thermal, crystallization, morphological, and mechanical properties of PVA/PEG (10 wt%) blend. *International Journal of Polymer Science, 2018*.

Feng, J., Fan, H., Zha, D.-a., Wang, L., & Jin, Z. (2016). Characterizations of the formation of polydopamine-coated halloysite nanotubes in various pH environments. *Langmuir, 32*(40), 10377–10386.

Fu, J., Chen, Z., Wang, M., Liu, S., Zhang, J., Zhang, J., … Xu, Q. (2015). Adsorption of methylene blue by a high-efficiency adsorbent (polydopamine microspheres): Kinetics, isotherm, thermodynamics and mechanism analysis. *Chemical Engineering Journal, 259*, 53–61.

Han, Y., Wu, X., Zhang, X., Zhou, Z., & Lu, C. (2016). Dual functional biocomposites based on polydopamine modified cellulose nanocrystal for Fe3+-pollutant detecting and autoblocking. *ACS Sustainable Chemistry & Engineering, 4*(10), 5667–5673.

Hu, D., Jiang, R., Wang, N., Xu, H., Wang, Y.-G., & Ouyang, X.-k. (2019). Adsorption of diclofenac sodium on bilayer amino-functionalized cellulose nanocrystals/chitosan composite. *Journal of Hazardous Materials, 369*, 483–493.

King, A. W., Mäkelä, V., Kedzior, S. A., Laaksonen, T., Partl, G. J., Heikkinen, S., … Cranston, E. D. (2018). Liquid-state nmr analysis of nanocelluloses. *Biomacromolecules, 19*(7), 2708–2720.

Konidari, M., Papadokostaki, K., & Sanopoulou, M. (2011). Moisture-induced effects on the tensile mechanical properties and glass-transition temperature of poly (vinyl alcohol) films. *Journal of Applied Polymer Science, 120*(6), 3381–3386.

Kubat, J., Rigdahl, M., & Welander, M. (1990). Characterization of interfacial interactions in high density polyethylene filled with glass spheres using dynamic-mechanical analysis. *Journal of Applied Polymer Science, 39*(7), 1527–1539.

Lönnberg, H., Fogelström, L., Berglund, L., Malmström, E., Hult, A., & Samir, M. A. S. A. (2008). Surface grafting of microfibrillated cellulose with poly (ε-caprolactone)–Synthesis and characterization. *European Polymer Journal, 44*(9), 2991–2997.

Lönnberg, H., Larsson, K., Lindstrom, T., Hult, A., & Malmström, E. (2011). Synthesis of polycaprolactone-grafted microfibrillated cellulose for use in novel bionanocomposites–influence of the graft length on the mechanical properties. *ACS Applied Materials & Interfaces, 3*(5), 1426–1433.

Mamun, A., Bazuin, C. G., & Prud'homme, R. E. (2015). Morphologies of various polycaprolactone/polymer blends in ultrathin films. *Macromolecules, 48*(5), 1412–1417.

Muiruri, J. K., Liu, S., Teo, W. S., Kong, J., & He, C. (2017). Highly biodegradable and tough polylactic acid–cellulose nanocrystal composite. *ACS Sustainable Chemistry & Engineering, 5*(5), 3929–3937.

Muiruri, J. K., Liu, S., Teo, W. S., Yeo, J. C. C., Thitsartarn, W., & He, C. (2018). Cavitation-crazing transition in rubber toughening of poly (lactic acid)-cellulose nanocrystal composites. *Composites Science and Technology, 168*, 12–19.

Muiruri, J. K., Liu, S., Yeo, J. C. C., Koh, J. J., Kong, J., Thitsartarn, W., … He, C. (2019). Synergistic toughening of poly (lactic acid)–cellulose nanocrystal composites through cooperative effect of cavitation and crazing deformation mechanisms. *ACS Applied Polymer Materials, 1*(3), 509–518.

Nagarajan, V., Mohanty, A. K., & Misra, M. (2016). Perspective on polylactic acid (PLA) based sustainable materials for durable applications: Focus on toughness and heat resistance. *ACS Sustainable Chemistry & Engineering, 4*(6), 2899–2916.

Nordgren, N., Carlsson, L., Blomberg, H., Carlmark, A., Malmström, E., & Rutland, M. W. (2013). Nanobiocomposite adhesion: Role of graft length and temperature in a hybrid biomimetic approach. *Biomacromolecules, 14*(4), 1003–1009.

Ohno, K., Morinaga, T., Koh, K., Tsujii, Y., & Fukuda, T. (2005). Synthesis of monodisperse silica particles coated with well-defined, high-density polymer brushes by surface-initiated atom transfer radical polymerization. *Macromolecules, 38*(6), 2137–2142.

Peng, Z., & Kong, L. X. (2007). A thermal degradation mechanism of polyvinyl alcohol/silica nanocomposites. *Polymer Degradation and Stability, 92*(6), 1061–1071.

Pereda, M., El Kissi, N., & Dufresne, A. (2014). Extrusion of polysaccharide nanocrystal reinforced polymer nanocomposites through compatibilization with poly(ethylene oxide). *ACS Applied Materials & Interfaces, 6*(12), 9365–9375.

Reiner, R. S., & Rudie, A. W. (2013). Process scale-up of cellulose nanocrystal production to 25 kg per batch at the Forest Products Laboratory. In M. T. Postek, R. J. Moon, A. W. Rudie, & M. A. Bilodeau (Eds.), *Production and applications of cellulose nanomaterials* (pp. 21–24). Peachtree Corners, GA: TAPPI Press.

Ryu, J. H., Messersmith, P. B., & Lee, H. (2018). Polydopamine surface chemistry: A decade of discovery. *ACS Applied Materials & Interfaces, 10*(9), 7523–7540.

Schuttlefield, J. D., & Grassian, V. H. (2008). ATR–FTIR spectroscopy in the undergraduate chemistry laboratory. Part I: Fundamentals and examples. *Journal of Chemical Education, 85*(2), 279.

Shang, Q., Liu, C., Hu, Y., Jia, P., Hu, L., & Zhou, Y. (2018). Bio-inspired hydrophobic modification of cellulose nanocrystals with castor oil. *Carbohydrate Polymers, 191*, 168–175.

Suhr, J., & Koratkar, N. (2006). Preventing interfacial slip in carbon nanotube polycarbonate composites. In *, Vol. 6169. Smart structures and materials 2006: Damping and isolation* (p. 616912). International Society for Optics and Photonics.

Suhr, J., & Koratkar, N. A. (2008). Energy dissipation in carbon nanotube composites: A review. *Journal of Materials Science, 43*(13), 4370–4382.

Yoo, Y., & Youngblood, J. P. (2016). Green one-pot synthesis of surface hydrophobized cellulose nanocrystals in aqueous medium. *ACS Sustainable Chemistry & Engineering, 4*(7), 3927–3938.

Zheng, T., & Pilla, S. (2020). Melt processing of cellulose nanocrystal-filled composites: Toward reinforcement and foam nucleation. *Industrial & Engineering Chemistry Research, 59*(18), 8511–8531.

Zhou, F., & Huck, W. T. (2006). Surface grafted polymer brushes as ideal building blocks for "smart" surfaces. *Physical Chemistry Chemical Physics, 8*(33), 3815–3823.